Symmetry breaking and gap opening in two-dimensional hexagonal lattices

2011 New J. Phys. 13 013026

(http://iopscience.iop.org/1367-2630/13/1/013026)

New Journal of Physics
The open-access journal for physics

Symmetry breaking and gap opening in two-dimensional hexagonal lattices

D Malterre[1,5], B Kierren[1], Y Fagot-Revurat[1], C Didiot[1], F J García de Abajo[2], F Schiller[3], J Cordón[4] and J E Ortega[3]

[1] Institut Jean Lamour, UMR 7198, Nancy-Université, BP 239, F-54506 Vandoeuvre-lès-Nancy, France
[2] Instituto de Óptica—CSIC, Serrano 121, 28006 Madrid, Spain
[3] Centro de Física de Materiales CSIC/UPV-EHU-Materials Physics Center, Manuel Lardizabal 5, E-20018 San Sebastián, Spain
[4] Dpto Física Aplicada I, Universidad del País Vasco, E-20018 San Sebastián, Spain
E-mail: daniel.malterre@ijl.nancy-universite.fr

New Journal of Physics **13** (2011) 013026 (9pp)
Received 31 July 2010
Published 19 January 2011
Online at http://www.njp.org/
doi:10.1088/1367-2630/13/1/013026

Abstract. The inhibition in wave propagation at band gap energies plays a central role in many areas of technology such as electronics (electron gaps), nanophotonics (light gaps) and phononics (acoustic gaps), among others. Here we demonstrate that metal surfaces featuring free-electron-like bands may become semiconducting by periodic nanostructuration. We combine scanning tunneling spectroscopy and angle-resolved photoemisssion to accurately determine the energy-dependent local density of states and band structure of the Ag/Cu(111) noble metal interface patterned with an array of triangular dislocations, demonstrating the existence of a 25 meV band gap that extends over the entire surface Brillouin zone. We prove that this gap is a general consequence of symmetry reduction in close-packed metallic overlayers; in particular, we show that the gap opening is due to the symmetry lowering of the wave vector group at the K point from C_{3v} to C_3.

[5] Author to whom any correspondence should be addressed.

Contents

1. Introduction

The electronic properties of solids depend on the chemical nature of the atomic constituents and their bonding. However, periodicity, i.e. symmetry, can play a fundamental role since the Bragg diffraction of the electron states can lead to gaps in the band structure. For example, the semiconducting character of silicon is a direct consequence of the symmetry of its Si crystal lattice. Similarly, the singular Fermi surface of graphene with linear dispersions associated with massless Dirac electrons at the K point of the surface Brillouin zone (SBZ) [1]–[3] also results from symmetry. Indeed, by changing the symmetry through interaction of a graphene plane with a substrate, the linear dispersion disappears and an energy gap takes place at the K point [4, 5]. This is of particular importance because, in fact, the role of graphene as a base material in nanoelectronics depends on the ability to engineer its semimetallic π bands in order to open semiconducting gaps, i.e. full gaps at the Fermi energy. On the other hand, electronic bands can be tailored and gaps can be induced by imposing a nanoscale super-periodicity with suitable symmetry, as is done in photonic crystals. It has been shown that hexagonal arrays of holes engraved in a dielectric yield gaps in the band diagrams for the directions of light propagation. The shape of the holes can have drastic consequences in the photonic band gap [6].

In this paper, we show that the existence or absence of gaps at the K point of the Brillouin zone (BZ) of a hexagonal lattice or superlattice is related to the symmetry of the crystal and more precisely to the symmetry of the wave vector group at the K point. The wave vector group is formed by the set of transformations leaving the wave vector unchanged. It depends on the position in the BZ. Such behavior is generic and can be invoked to explain different properties such as gaps not only in the electron band structure but also in the band diagrams for light propagation in photonic crystals. In the latter example, the change of hole shape from circular to elliptical that leads to the opening of a gap at the K point is accompanied by a change of symmetry at this particular point. In this paper, we discuss in detail the role of symmetry in gap opening, in the framework of the nearly free electron approach, which is the simplest and most intuitive model of the electronic structure.

The free-electron-like framework is well suited for describing the electron band structure of the Shockley states of noble metal (111) surfaces. The super-periodic potential associated with surface reconstruction can be considered as a small perturbation revealing the relation between symmetry and electronic properties. The Ag/Cu(111) surface is a prototype scenario to study the transformation of the band structure due to symmetry changes in a nanoscale reconstruction [7, 8]. When deposited at low temperature, the Ag monolayer exhibits a $\sim 8 \times 8$(Ag)-on-9×9(Cu) coincidence lattice. Annealing to 300 K allows the system to relax, creating a $\sim 9.5 \times 9.5$ network of triangular dislocation loops within the Cu(111) substrate [9, 10]. As a

consequence, the weakly scattering, sixfold Moiré pattern turns into a stronger, threefold-symmetric, repulsive potential superlattice in the dislocation network [11, 12]. Here we show that such transformation allows one to lift the degeneracy of the K point of the surface band structure, where a 25 meV gap is opened. We show that the gap opening and the evolution of the local density of states (LDOS) can be simply explained by symmetry. The energy gap and the LDOS have been obtained from angle-resolved photoemission spectroscopy (ARPES) and scanning tunneling spectroscopy (STS). We show that group theory predicts a gap opening at this K point, but is also able to give a satisfactory description of the LDOS associated with the high symmetry points of the BZ.

2. Technical details

Scanning tunneling microscopy (STM) and STS experiments were performed using a 5 K-Omicron STM. The $\mathrm{d}I/\mathrm{d}V$ maps (and spectra) were recorded at 5 K in the open feedback loop mode using the lock-in technique with a bias modulation of 3 meV rms at 700 Hz. Before transferring to the STM cryostat at 5 K, the Ag monolayer was evaporated at 150 K on the clean Cu(111) crystal and then annealed to 350 K. This process leads to the sharp $\sim(9.5 \times 9.5)$ hexagonal lattice of triangular dislocations. Annealing the Ag/Cu(111) monolayer at 350 K is necessary for eliminating the unfavorable on-top positions of the low-temperature Moiré lattice by creating triangular dislocation loops within the substrate [9]. This process implies the removal of five Cu atoms from the topmost Cu(111) plane and the shift of another ten substrate atoms to hcp positions, leaving a triangular dislocation loop around. A defect-free Ag(111) layer is then observed to wet the nanostructured substrate. The angle-resolved photoemission experiments were performed with a Scienta 200 high-resolution hemispherical analyzer at the Synchrotron Radiation Center in Stoughton (Wisconsin) and were reported in [7]. The sample was illuminated with monochromatized photons of $h\nu = 21$ eV and measured at room temperature in order to populate states above the Fermi energy.

3. Results and discussion

In figure 1, we investigate the electronic surface band structure for a two-dimensional (2D) superlattice potential based on symmetry arguments. The top panel describes real lattices for hexagonal arrays of an empty crystal (b), circular (c) and triangular (d) potentials and the corresponding BZ in reciprocal space (a), whereas the bottom panels represent the respective band structure along the ΓM and ΓK directions. The unit cell in real space is shown in red. Note that the six points at the corner of the hexagonal BZ are not the same because they are not related by a reciprocal vector. Then, there are two inequivalent points K and K'. However, as the wave vector at K' corresponds to the opposite value at K, the two associated states are related by time reversal and have the same energy. Firstly, let us consider the empty lattice approximation ($V \equiv 0$). The space group is the 2D group $P6mm$ or C_{6h}^{1}. For the electronic properties, it is useful to consider the small groups (i.e. the group of the wave vector at the high symmetry $\vec{k}$ points of the BZ). At the Γ point, the symmetry group of the wave vector is C_{6v} and the lowest energy band that corresponds to the plane wave state $|\vec{k} = 0\rangle$ is associated with the totally symmetric irreducible representation A_{1g}. At the M point (C_{2v} symmetry), the lowest energy level is twofold ($|\vec{k}_M\rangle$ and $|\vec{k}_M - \vec{G}_1\rangle$) and the

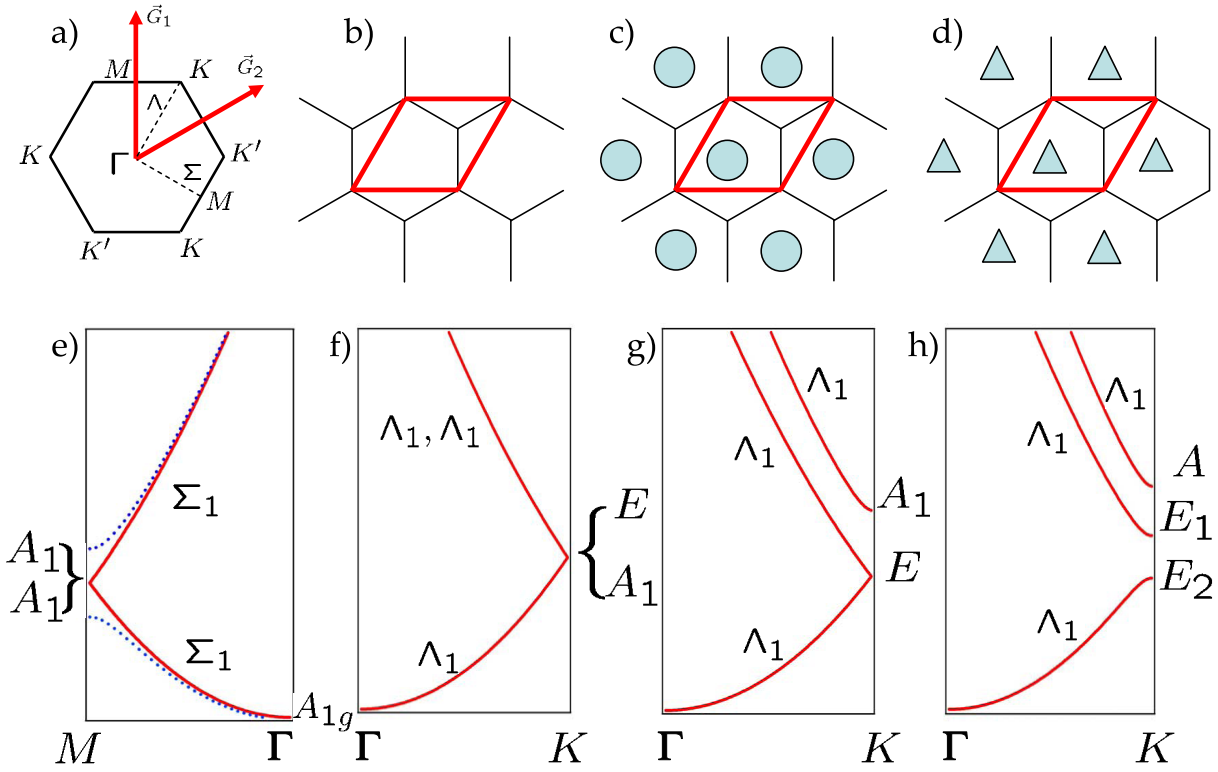

Figure 1. (a) The BZ of the hexagonal lattice with the high symmetry points and directions. Lattices for the empty crystal (b) and for circular (c) and triangular (d) reconstructions. Band dispersions in the ΓM and ΓK directions for the empty lattice (e, f) and in the ΓK direction for circular (g) and triangular (h) reconstructions. The effect of a finite potential on the band dispersion in the ΓM direction is illustrated by the blue dotted line in (e).

corresponding 2D representation $\Gamma_M^{(1)}$ can be decomposed on the irreducible representations of C_{2v}: $\Gamma_M^{(1)} = 2A_1$.

A finite potential will lead to two non-degenerate states $(|\vec{k}_M\rangle \pm |\vec{k}_M - \vec{G}_1\rangle)/\sqrt{2}$ separated in first order by the corresponding Fourier component $2|V_{\vec{G}_1}|$, as illustrated by the blue dotted line in figure 1(e). At the K point, the symmetry group is C_{3v} and the lowest level is a triplet spanned by the three states $|\vec{k}_K\rangle$, $|\vec{k}_K - \vec{G}_1\rangle$ and $|\vec{k}_K - \vec{G}_2\rangle$. The 3D reducible representation associated with this energy level at K can be decomposed into the irreducible representations of C_{3v}: $\Gamma^0 = A_1 \oplus E$, where A_1 is the totally symmetric representation and E is a 2D representation. Therefore, a finite potential with the same symmetry as, for example, that generated by a circular reconstruction leads to a singlet (A_1 representation) and a doublet (E representation). This is illustrated in figure 1(g) and confirmed by calculation. Using perturbation theory one can show that for a positive Fourier component V_G of the potential, the K point (E_K energy) features a lower-energy, doubly degenerate state associated with E ($E = E_K - V_G$), plus a higher-energy, non-degenerate state associated with the A_1 symmetry ($E = E_K + 2V_G$). Therefore, for a repulsive superlattice potential with hexagonal symmetry, no gap appears at K.

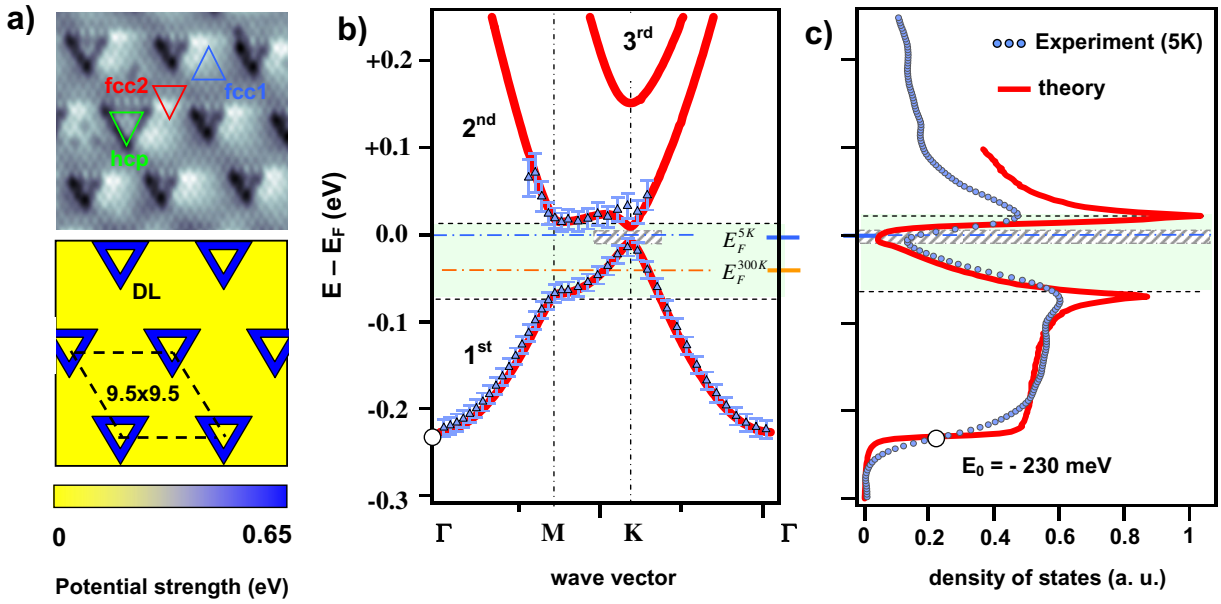

Figure 2. (a) STM topographic image evidencing the triangular dislocation network of Ag/Cu(111) (top) and modelization of the electron potential corresponding to the triangular dislocation loop (bottom). (b) Calculated band dispersions (solid red lines) and ARPES experimental data recorded at room temperature and shifted to take into account the rigid shift between 300 K and 5 K ([7]). (c) Calculated density of states and 5K-STS spectrum averaged over the surface. In (b) and (c), the green and blue shadings represent the M and K gaps, respectively.

For the lattice of triangles, the symmetry is lowered, the space group is $P3m1$ or C_{3v}^1. The group at Γ is C_{3v}, at M, C_{1h} and at K, C_3. The lowering of symmetry at K from C_{3v} (circles) to C_3 (triangles) is very similar to the change from graphene to hexagonal BN and has a consequence of fundamental nature. As energy degeneracy is due to the existence of non-commutative symmetry operators, the change from the non-abelian group C_{3v} to the abelian one C_3 should lead to the disappearance of band crossing at the K point. This is confirmed by the representation of decomposition at the K point, which leads to three singlets A, E_1 and E_2 as depicted in figure 1(h). It is interesting to note that the table of characters of the C_{3v} group shows that the E_1 and E_2 are complex conjugated, indicating that these two representations are related by time reversal [13]. It does not mean that they are degenerate at the same point, since the reversal of time transforms a wave vector into its opposite. As a consequence, the state associated with E_1 at the K point transforms into the state associated with E_2 at the K' point. At the M point, as the wave vector group does not change, no modification is expected. To conclude, the lowering of symmetry leads to an additional energy gap at the K point in the band structure, no matter what the sign of the superlattice potential V is.

In figure 2(a), we show an STM topographic image of the Ag/Cu(111) surface. Two fcc-like (fcc1 and fcc2) areas and one hcp-like (on top of the triangle hcp) area can be identified. The schematic triangular lattice also depicted in figure 2(a) models the network of triangular dislocation loops within the Cu(111) substrate. Surface bands are calculated by solving an

effective one-electron Schrödinger equation in this modelled potential:

$$(\nabla^2 + k^2 - 2m^* V)\phi = 0 \tag{1}$$

in two dimensions, where $m^* = 0.42m_0$ stands for the effective mass of the Ag/Cu(111) measured in photoemission. The periodic potential mimicking the triangular dislocation is expanded in 2D plane waves. The potential is set to zero (the surface-state band minimum) everywhere except in the regions defined by pairs of triangles that share their centers, where it takes a value of 650 meV in order to fit the measured surface bands. The side of the inner (outer) triangle is 5.78 (14.44) Å, as deduced from the STM images. The lattice constant (24.28 Å) corresponds to a 9.5×9.5 reconstruction. The LDOS is obtained by direct integration of the resulting bands over the 2D wave vector. Electron bands of such a network are measured by ARPES in figure 2(b). Experiments have been performed at room temperature, making it possible to probe thermally occupied states 50 meV above the Fermi energy [12]. Data points in figure 2(b) were obtained from standard line fits of individual energy distribution curves (EDCs), using two Lorentzian functions multiplied by the Fermi Dirac function and convoluted with a Gaussian line to account for the experimental resolution [7]. This procedure allows additional visualization of peaks within $\pm 2k_B T$ above the Fermi edge. Such an analysis evidences a 100 meV gap at the M point and a small one (25 meV) at the K point. In fact, at room temperature, the K-point gap is in the unoccupied part of the spectrum, as shown by the position of the Fermi energy at 300 K (horizontal dashed line in figure 2(b)). It is important to note that surface bands in noble metals shift by ~50 meV to lower energy when going from 300 to 20 K [14]. This is also the case for the Ag/Cu(111) system, where an almost rigid shift as a function of temperature is observed [12], which drives the K band gap to the Fermi energy at 5 K, as proved by STS in figure 2(c). Therefore, the band dispersion in figure 2(b) has been shifted by -35 meV in order to compare with the low-temperature STS spectrum. The red lines fit the ARPES data across the entire BZ. They represent the band structure calculation obtained from the model potential reconstruction illustrated in figure 2(a), which was presented and discussed elsewhere [12]. The potential inside the triangular loop is the only adjustable parameter in this model, which is fixed at $V = 650$ meV in order to fit the measured surface bands. The calculation allows us to determine the gap size (25 meV) at the K point of the superlattice band structure. In figure 2(c), we compare the density of states calculated with the same model (red spectrum), with the average density of states measured by STS at 5 K (dotted spectrum). The STS spectrum exhibits a strong depletion between two peaks associated with the gap edges at the M point. In the average STS spectrum, it is not possible to see the signature of the additional gap at the K point. But, as mentioned above, the triangular reconstruction of Ag/Cu(111) exhibits three inequivalent symmetry positions. The STS spectra recorded on these three regions show a strong depletion close to the Fermi energy with a small shoulder at $E \sim -40$ meV, close to the energy of the calculated K gap, visible on the STS spectra recorded in the hcp and fcc1 areas (figure 3(a)). Therefore, STS, photoemission and the model exhibit excellent agreement, proving the presence of the M and K point band gaps spanning the entire BZ at the Fermi energy. Therefore, in the Ag/Cu(111) system, the gap position can be driven by changing the system temperature, making the noble metal surface effectively semiconducting at 5 K and metallic at room temperature.

Below 150 meV, the LDOS in the triangular hcp region is smaller than the LDOS in the two fcc regions. Above 150 meV, a strong increase is observed on top of the triangular dislocation loops. In figure 3(b), we present $(\mathrm{d}I/\mathrm{d}V)$ spectroscopy maps recorded at energies

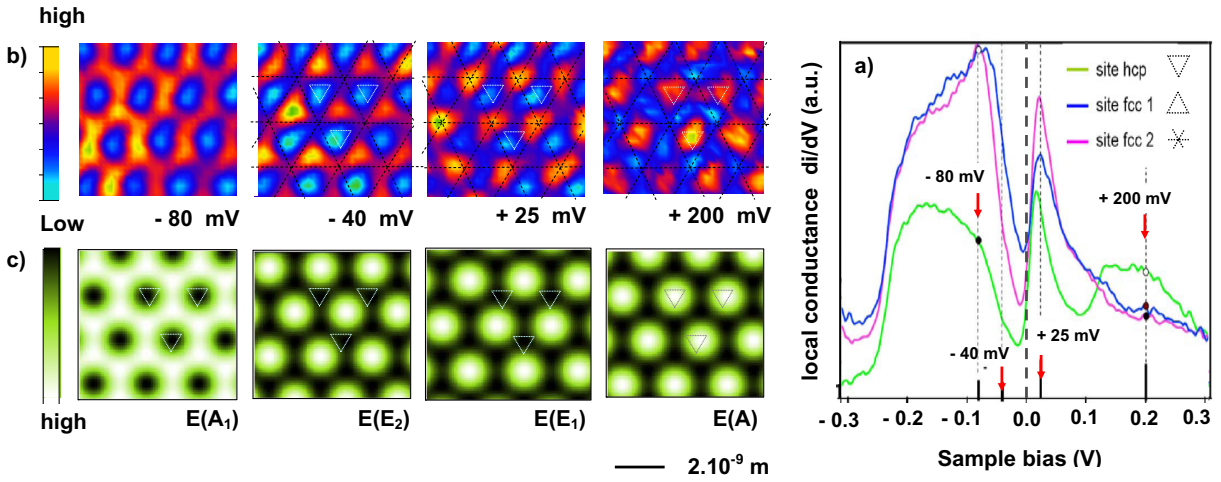

Figure 3. (a) Experimental STS spectra recorded on the different regions: the two fcc regions and the triangular hcp region. (b) STS spectroscopic maps recorded at energies corresponding to the localization of the LDOS in the different regions. (c) LDOS simply obtained from group theory and associated with the basis functions of the irreducible representations of the high symmetry M and K points. The white triangles in the experimental and calculated maps represent the triangular dislocation loops.

−80, −40, 22 and 200 meV, as indicated by arrows in figure 3(a). Dephasing behavior in the electron density maps has been shown to reflect band gaps in such nearly-free-electron-like systems [15, 16]. At −80 meV, LDOS maxima correspond to the two fcc regions in the lattice. At −40 meV and +22 meV, the LDOS maxima are located in the fcc1 and fcc2 regions, respectively. This dephasing is strong support for the existence of a band gap at the K point. Around +200 meV, the maxima of the LDOS are found in the triangles. Such localizations of the LDOS should reflect the symmetry of the band states at the K and M points where the Bragg mechanism induces electron standing waves. To prove this statement, we have compared these experimental maps with the calculated LDOS obtained from symmetry. Indeed the basis states of the irreducible representations, in the first order of perturbation theory, can be obtained without solving the Schrödinger equation by using the projector technique of group theory based on the characters of irreducible representations [13]. The projector on the basis based on the states of the irreducible representation B is given by

$$\mathcal{P}^{(B)} = \frac{\ell_B}{h} \sum_R \chi^{(B)}(R)^* P_R,$$

where $\chi^{(B)}(R)$ is the character of the representation B for the symmetry operation R, h is the number of symmetry elements, ℓ_B is the dimension of B and P_R is the symmetry operator corresponding to R. Then, by applying $\mathcal{P}^{(B)}$ on a plane wave, one obtains the wave function corresponding to the B irreducible representation. Therefore, by projecting the basis states of the free electron representations at the M and K points on the irreducible representations of the relevant wave vector groups, it is possible to deduce the Bloch waves and the corresponding density at these high symmetry points without solving the Schrödinger equation. At the K point,

for the totally symmetric representation A, the state is

$$\Psi^{(A)}(\vec{r}) = \frac{1}{\sqrt{3}}\left[e^{i\vec{k}_K\cdot\vec{r}} + e^{(i\vec{k}_K-\vec{G}_1)\cdot\vec{r}} + e^{i(\vec{k}_K-\vec{G}_2)\cdot\vec{r}}\right], \tag{2}$$

whereas for the E_1 and E_2 representations we have

$$\begin{aligned}\Psi^{(E_1)}(\vec{r}) &= \frac{1}{\sqrt{3}}\left[e^{i\vec{k}_K\cdot\vec{r}} + \varepsilon\ e^{(i\vec{k}_K-\vec{G}_1)\cdot\vec{r}} + \varepsilon^*\ e^{i(\vec{k}_K-\vec{G}_2)\cdot\vec{r}}\right],\\ \Psi^{(E_2)}(\vec{r}) &= \frac{1}{\sqrt{3}}\left[e^{i\vec{k}_K\cdot\vec{r}} + \varepsilon^*\ e^{(i\vec{k}_K-\vec{G}_1)\cdot\vec{r}} + \varepsilon\ e^{i(\vec{k}_K-\vec{G}_2)\cdot\vec{r}}\right],\end{aligned} \tag{3}$$

with $\varepsilon = \exp 2\pi i/3$. The electron density corresponding to these representations at the K point can be obtained by taking the square of these wave functions. To simulate a density map at a given energy that could be compared with the STS images as in figure 3, it is necessary to sum the contribution of the six corners (K and K' points) of the hexagonal BZ. The agreement between experimental and calculated maps (figures 3(b) and (c)) suggests that the −80 eV and −40 eV maps correspond to the low gap edges at the M and K points, respectively, whereas the +20 meV and +200 meV maps are associated with the states at the K points with E_1 and A symmetry, respectively.

4. Conclusion

In summary, we have shown that the triangular potential associated with the dislocation network in the Ag/Cu(111) system lowers the sixfold symmetry of the surface and opens a full band gap in an otherwise metallic surface. The existence of a gap is related to the dimension of the irreducible representation of the small or wave vector group at the relevant high symmetry points of the BZ. For such a hexagonal lattice, symmetry lowering leads to symmetry change at the K point whereas the symmetry at the M point is not modified. Moreover, projectors provide an elegant way of obtaining the electron density at these high symmetry points. The virtuality of symmetry breaking has been proposed for the graphene system, but within the atomic unit cell [4]. In fact, breaking the carbon sublattice symmetry (e.g. with strongly interacting fcc substrates) opens a gap at the K point of the graphene band structure [4]. We show in this paper that a surface gap can be induced by the superlattice potential of a reconstruction. The symmetry-induced superlattice gaps may have advantages with respect to atomic scale gaps. Superlattice gaps are usually smaller than atomic lattice gaps, and are potentially easier to drive by nanostructuration of the surface.

Acknowledgments

This work was supported in part by the Spanish MICINN (MAT2007-66050, MAT2007-63083 and Consolider NanoLight.es), the EU (NMP4-SL-2008-213669-ENSEMBLE), the Basque Government (IT-257-07) and the Centre National de la Recherche Scientifique (CNRS).

References

[1] Zhou Y *et al* 2006 *Nat. Phys.* **2** 595
[2] Bostwick A, Ohta T, Seyller T, Horn K and Rotenberg E 2006 *Nat. Phys.* **3** 36

[3] Sprinkle M *et al* 2009 *Phys. Rev. Lett.* **103** 226803
[4] Zhou S Y *et al* 2007 *Nat. Mater.* **6** 770
[5] Bostwick A, Ohta T, McChesney J L, Emtsev K V, Seyller T, Horn K and Rotenberg E 2007 *New J. Phys.* **9** 385
[6] Quiñónez F *et al* 2006 *Opt. Exp.* **14** 4873
[7] Schiller F, Cordón, Vyalikh D, Rubio A and Ortega J E 2005 *Phys. Rev. Lett.* **94** 016103
[8] Bork J, Wahl P, Diekhöner L and Kern K 2009 *New J. Phys.* **11** 113051
[9] Meunier I, Tréglia G, Gay J-M, Aufray B and Legrand B 1999 *Phys. Rev.* B **59** 10910
[10] Bendounan A, Cercellier H, Fagot-Revurat Y, Kierren B, Yurov V and Malterre D 2003 *Phys. Rev.* B **67** 165412
[11] Bendounan A *et al* 2006 *Phys. Rev. Lett.* **96** 029701
Bendounan A *et al* 2006 *Phys. Rev.* B **72** 075407
[12] Schiller F, Cordón J, Vyalikh D, Rubio A and Ortega J E 2006 *Phys. Rev. Lett.* **96** 029702
[13] Tinkham M 1964 *Group Theory and Quantum Mechanics* (New York: McGraw-Hill)
[14] Paniago R, Matzdorf R, Meister G and Goldman A 1995 *Surf. Sci.* **336** 113
[15] Didiot C, Fagot-Revurat Y, Pons S, Kierren B, Chatelain C and Malterre D 2006 *Phys. Rev.* B **74** 081404
[16] Malterre D *et al* 2007 *New J. Phys.* **9** 391